Parton distributions for the pion extracted from Drell-Yan and prompt photon experiments

P. J. Sutton and A. D. Martin
Department of Physics, University of Durham, Durham, DH1 3LE, England

R. G. Roberts
Rutherford Appleton Laboratory, Chilton, Didcot, Oxon, OX11 0QX, England

W. J. Stirling
Department of Physics, University of Durham, Durham, DH1 3LE, England
(Received 4 September 1991; revised manuscript received 23 September 1991)

We determine the parton distributions of the pion from a consistent next-to-leading-order analysis of several high-statistics $\pi^{\pm}N$ experiments including both Drell-Yan and prompt photon production.

PACS number(s): 12.38.Qk, 12.38.Bx, 13.85.Qk, 14.40.Aq

I. INTRODUCTION

The parton distributions of the nucleons are now well determined by global analyses of a whole range of precise data for deep-inelastic lepton-nucleon scattering and for Drell-Yan and prompt-photon production. The most recent analyses [1] include the next-to-leading-order (NLO) QCD contributions. However, much less is known about the parton distributions of other hadrons.

There now exist data from several high-statistics experiments on pion-nucleon and pion-nucleus collisions. These experiments include both Drell-Yan and prompt photon production. If we assume that the nucleon distributions are precisely known, these data can be used to determine the parton distributions of the pion. In the past, several attempts [2–6] have been made to extract such information either from subsets of the data or from earlier measurements of the processes. Until now, however, there has been no simultaneous QCD analysis at next-to-leading order of all of the recent high-precision pion data. In addition to being of interest in their own right and to compare with the nucleon distributions, the parton distributions of the pion are needed for checking the predictions of lattice QCD and will be valuable for estimates of processes at the DESY ep collider HERA based on the vector-meson-dominance model of the photon, albeit with the vector meson approximated by a pseudoscalar.

Here we perform a NLO analysis of the Drell-Yan and prompt photon πN data. Since the nucleon distributions are much better determined than those of the pion, it is sufficient to fix on a single set of partons for the proton and to use the πN data to determine only the structure of the pion. We work in the modified minimal subtraction ($\overline{\rm MS}$) scheme and we use the Harriman-Martin-Roberts-Stirling set B [HMRS(B)] of parton distributions of the proton [1]. Hence we take the same value of $\Lambda_{\overline{\rm MS}}$ (with four flavors) as obtained by HMRS, namely

$$\Lambda^{(4)}_{\overline{\rm MS}}=190\ \text{MeV}\ . \tag{1}$$

The quark distributions are defined in the universal $\overline{\rm MS}$ factorization scheme. We use the following parametrization to describe the parton distributions of the pion (π^-) at $Q^2=Q_0^2=4\ \text{GeV}^2$:

$$xV_\pi = A_V x^{\alpha}(1-x)^{\beta}\ , \tag{2}$$

$$xS_\pi \equiv 2x(u+\bar{d}+\bar{s}) = A_s(1-x)^{\eta_s}\ , \tag{3}$$

$$xg = A_g(1-x)^{\eta_g}\ , \tag{4}$$

where $V_\pi=\bar{u}_V=d_V$ and A_V is determined in terms of α and β by the flavor content of the pion. A_s is taken as a free parameter, so that A_g is determined by η_g and the momentum sum rule. We make the assumption that at $Q^2=Q_0^2$ the pion sea is SU(3) symmetric. That is, we assume

$$u=\bar{d}=\bar{s}\ . \tag{5}$$

Suppressing the strange-quark distribution relative to an SU(2)-symmetric sea, as, for example, in the proton, would have little effect given the fairly large uncertainty in the sea distribution. The charm distribution of the pion is generated through the evolution equations assuming that the charm quark is massless and that $c(x,Q_0^2)=0$. There are thus a total of five free parameters to be determined by the data (α, β, A_s, η_s, and η_g). We find that the valence quark distributions of the pion are primarily determined by the Drell-Yan data and that the gluon distribution of the pion is mainly constrained by the π^+ prompt photon production process, $\pi^+p\to\gamma X$; the process $\pi^-p\to\gamma X$ being dominated by $q\bar{q}$ annihilation [5].

II. VALENCE DISTRIBUTIONS AND THE DRELL-YAN DATA

The dominant QCD process contributing to Drell-Yan production, $\pi^{\pm}N\to\mu^+\mu^-X$, is $q\bar{q}$ annihilation, and, hence, in principle, these data determine both the valence- and the sea-quark distributions of the pion. Unfortunately at present there is no available experimental

information at sufficiently small x_π ($x_\pi \lesssim 0.2$) to allow an unambiguous determination of the sea-quark distribution of the pion. However, this ambiguity does not lead to appreciable uncertainties in the determination of the valence (and gluon) distributions from data at larger x_π values.

Recently the calculation of the Drell-Yan cross section up to order $\alpha_s^2(Q^2)$ [7] has been completed, although the differential form is not available. Here we work consistently at next-to-leading order and we therefore use the expressions of Kubar *et al.* [8] suitably modified to the $\overline{\text{MS}}$ regularization scheme (as given in Appendix A). In order to compare theory with experiment we calculate the double differential cross section

$$\frac{d^2\sigma}{dx_F d\sqrt{\tau}} ,$$

where

$$x_F = x_\pi - x_N \quad \text{and} \quad \tau = x_\pi x_N = \frac{M^2}{s} , \tag{6}$$

x_π and x_N are, at leading order, the Bjorken x variables of the pion and target nucleon, respectively, M is the invariant mass of the muon pair, and $\sqrt{s}$ is the center-of-mass energy.

In calculating the cross sections we use the full next-to-leading-order expressions (with no exponentiated terms) and the "natural" choice of scale $Q^2 = M^2$. We multiply our theoretical cross sections by an extra free parameter K' to allow for higher-order QCD contributions to the cross section as well as uncertainties in the overall experimental normalization. It should be noted that there exists some correlation between this factor and the parameters α and β. Fortunately our fits seem to indicate values of K', α, and β that appear very reasonable.

We analyze two independent sets of high-statistics Drell-Yan data obtained from a π-beam incident on a tungsten target, $\pi^- W \to \mu^+\mu^- X$, by the NA10 and E615 Collaborations. To extract the pion distributions from these data it is necessary to allow for the presence of nuclear effects. As mentioned earlier, we use the HMRS(B) distributions for the proton. This means that we need to correct for the fact that the Drell-Yan data were taken on a heavy nuclear target. We do this by multiplying the parametrized cross section by a smooth function

$$R = \frac{d\sigma(\pi W \to \mu^+\mu^- X)}{d\sigma(\pi D \to \mu^+\mu^- X)} , \tag{7}$$

corrected for isoscalarity effects. It is expected from QCD factorization that R will depend only on the target x_N, and not x_π. This is consistent with the experimental measurements of R. The observed values of R [9] are shown in Fig. 1 as a function of x_N, and are well described by the straight line

$$R = -0.55 x_N + 1.1 . \tag{8}$$

We use this form in the results presented here, although we estimate the uncertainty due to nuclear effects by correcting the predictions with other forms for R, including $R = 1$.

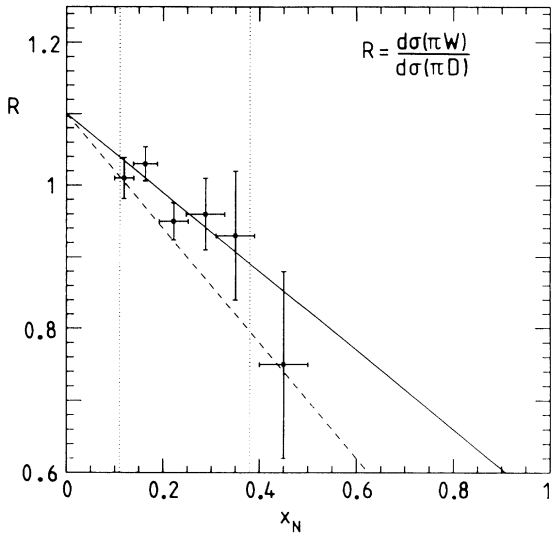

FIG. 1. The ratio $d\sigma(\pi^- W \to \mu^+\mu^- + X)/d\sigma(\pi^- D \to \mu^+\mu^- + X)$ as a function of x_N. The data points are from Ref. [9]. The solid straight line is $R = -0.55x_N + 1.1$, the dashed one is $R = -0.8x_N + 1.1$. The vertical dotted lines indicate the range of x_N values spanned by the NA10 data included in our fit.

The CERN NA10 experiment [10,11] has accumulated the highest-statistics Drell-Yan data (155 000 events). This experiment measured the differential cross section at two separate beam energies, 194 GeV/c and 286 GeV/c, for a π^- beam on a tungsten target. We choose to perform a fit to the combined data of both energies in a mass range $4.16 < M < 8.34$ GeV/c^2. This region, between the J/ψ and the Υ resonances, is where the relative errors are smallest and also where NLO QCD is most in agreement with the NA10 data. At higher values of $\sqrt{\tau}$ there is some deviation of the data from the predictions of our QCD analysis. The reasons for this are not clear. We avoid these problems by cutting out this high-$\sqrt{\tau}$ region. In addition to this restriction we reject the lowest bin at both energies because of possible background contamination [10]. The regions we are fitting are thus: $0.24 < \sqrt{\tau} < 0.42$ at 194 GeV/c and $0.21 < \sqrt{\tau} < 0.36$ at 286 GeV/c. We also discount data points with $x_F < 0$ because of possible reinteraction effects.

To begin we compare the partons determined from several different fits to these data in which η_g is kept fixed at $\eta_g = 2.1$. The Drell-Yan cross section is not very sensitive to this parameter and, as we shall see in the next section, η_g is well determined by the prompt photon data; $\eta_g = 2.1 \pm 0.4$. We first vary the parameters α, β, K'_{194}, and K'_{286} to achieve an optimum fit to the CERN NA10 Drell-Yan data. Set 1 of Table I is obtained by fitting only to the Drell-Yan data with $x_\pi > 0.35$ where the pion sea is irrelevant. The remainder of the fits in Table I include the Drell-Yan data down to $x_\pi \simeq 0.2$ where the pion sea cannot be neglected. Rather than assume a form for the sea quarks we perform a range of fits in which the

TABLE I. The values of the parton parameters of the pion obtained by fitting to the NA10 data of Ref. [10] for various choices of the sea-quark distribution. Set 1 shows the effect of fitting only to data points for which $x_\pi > 0.35$. Fits 2 to 5 show the effect of steadily increasing the sea from one which carries 5% of the pion's momentum at $Q^2 = Q_0^2$, to one which carries 20%. The parameters in parentheses are held fixed during each fit.

Fit	α	β	A_s	η_s	η_g	K'_{194}	K'_{286}	χ^2/No. of data
1	0.65	1.07			(2.1)	1.30	1.38	48/52
2	0.59	1.08	(0.3)	(5.0)	(2.1)	1.39	1.48	157/62
3	0.61	1.08	(0.6)	(5.0)	(2.1)	1.39	1.48	58/62
4	0.64	1.08	(0.9)	(5.0)	(2.1)	1.33	1.41	54/62
5	0.61	1.02	(1.2)	(5.0)	(2.1)	1.34	1.41	52/62

sea carries an increasing fraction of the pion's momentum. Figure 2 shows the various sea distributions that we consider and in a later plot (Fig. 10) we will show the effect of their contribution to the overall quark distribution. It can be seen from Table I that the value of β is hardly affected until the sea distribution becomes quite large ($\langle xS_\pi \rangle \sim 0.2$). The value of α is, as should be expected, more sensitive, but for those sea distributions for which a good description is obtained (fits 3–5) the value of α changes only by 0.03 and, moreover, is comparable with the value obtained in fit 1. The valence parameters shown in Table I can be seen to be in good agreement with those of Ref. [11].

Sets 6 and 7 (Table II) show the effect of varying the nuclear function R. Fit 6 is a repeat of fit 4 but with no correction applied for the effect of the heavy nucleus; that is, with R of (7) replaced by $R = 1$. Fit 7 shows the effect of an extreme nuclear correction, described by $R = -0.8x_N + 1.1$ and shown by the dashed line of Fig. 1. These two fits show the sensitivity of the parameters to nuclear effects, although, as can be seen from Fig. 1, they more than span the range of "nuclear" uncertainty.

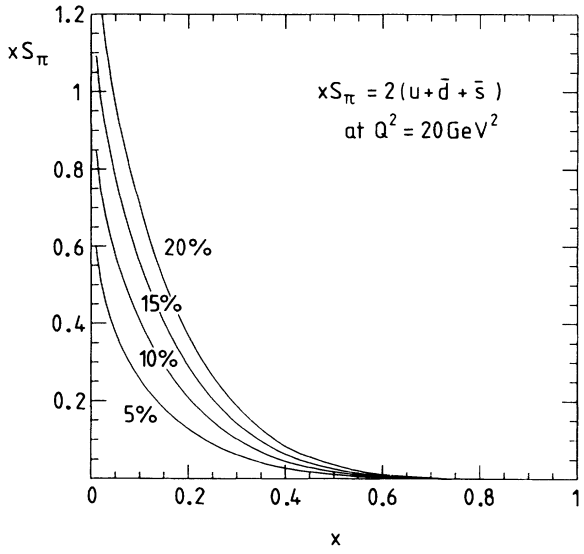

FIG. 2. The range of sea distributions, $xS_\pi = 2x(u + \bar{d} + \bar{s})$, at $Q^2 = 20$ GeV^2 that we include in our fits to the NA10 and E615 Drell-Yan data. The distributions carry 5%, 10%, 15%, and 20% of the pion's momentum at $Q^2 = Q_0^2 = 4$ GeV^2.

For comparison, we next analyze the data of the Fermilab E615 experiment [6] (36 000 events). These data are also obtained from a π^- beam on a tungsten target and so we can use the same function R as we used in the fits 1 to 5. The E615 data that we study are in the mass range $4.03 < M < 8.53$ GeV/c^2 for a beam energy of 252 GeV. This corresponds to the range $0.185 < \sqrt{\tau} < 0.392$. Sets 8–12 of partons listed in Table III are obtained by fitting to these data (and can be compared with sets 1–5 of Table I obtained from the NA10 data). We find that the E615 data for the two highest $\sqrt{\tau}$ bins in this analysis lie consistently above the best-fit curve and so we have repeated the fits omitting these two bins; that is to say we fit the range $0.185 < \sqrt{\tau} < 0.346$. The results are listed in Table IV.

Finally we repeat the fit to both the NA10 and E615 data with the valence parameters fixed at the values obtained from the analysis of the other data set. The only free parameters are thus the overall normalization K' fac-

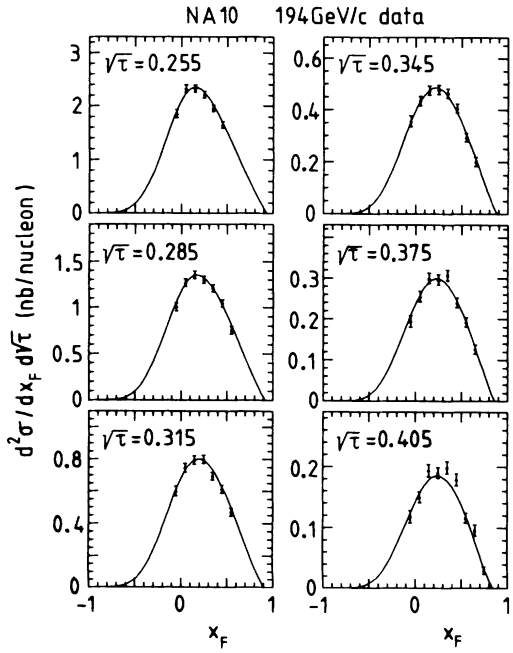

FIG. 3. Drell-Yan data from the NA10 Collaboration [10] for 194 GeV/c π^- on W, together with their description in terms of the NA10 parton distributions of Table VII. The points with $x_F < 0$ are not included in the fit.

TABLE II. Parameters obtained in fits to the NA10 data using two extreme choices for the function R. Set 6 shows the effect of omitting nuclear effects, $R=1$, whereas set 7 is obtained from assuming a very pronounced nuclear effect, $R=-0.8x_N+1.1$. The parameters in parentheses are held fixed during each fit.

Fit	α	β	A_s	η_s	η_g	K'_{194}	K'_{286}	χ^2/No. of data
6	0.65	1.05	(0.9)	(5.0)	(2.1)	1.29	1.38	58/62
7	0.62	1.06	(0.9)	(5.0)	(2.1)	1.44	1.51	82/62

TABLE III. Parameters obtained by fitting to the E615 data of Ref. [6] (inclusive of the two high $\sqrt{\tau}$ bins) using various input sea-quark distributions. Set 8 shows the effect of fitting only to data points for which $x_\pi > 0.35$. Fits 9 to 12 show the effect of steadily increasing the sea from one which carries 5% of the pion's momentum at $Q^2=Q_0^2$, to one which carries 20%. The parameters in parentheses are held fixed during each fit.

Fit	α	β	A_s	η_s	η_g	K'_{252}	χ^2/No. of data
8	0.59	1.13			(2.1)	1.23	83/69
9	0.63	1.16	(0.3)	(5.0)	(2.1)	1.18	90/78
10	0.66	1.16	(0.6)	(5.0)	(2.1)	1.11	91/78
11	0.67	1.15	(0.9)	(5.0)	(2.1)	1.07	91/78
12	0.71	1.16	(1.2)	(5.0)	(2.1)	1.00	92/78

TABLE IV. Parameters obtained by fitting to the E615 data of Ref. [6] (exclusive of the two high $\sqrt{\tau}$ bins) using various input sea-quark distributions. Set 13 shows the effect of fitting only to data points for which $x_\pi > 0.35$. Fits 14 to 17 show the effect of steadily increasing the sea from one which carries 5% of the pion's momentum at $Q^2=Q_0^2$, to one which carries 20%. The parameters in parentheses are held fixed during each fit.

Fit	α	β	A_s	η_s	η_g	K'_{252}	χ^2/No. of data
13	0.58	1.11			(2.1)	1.20	43/52
14	0.59	1.15	(0.3)	(5.0)	(2.1)	1.22	50/61
15	0.66	1.18	(0.6)	(5.0)	(2.1)	1.11	50/61
16	0.64	1.14	(0.9)	(5.0)	(2.1)	1.11	52/61
17	0.67	1.15	(1.2)	(5.0)	(2.1)	1.05	53/61

TABLE V. Fits 18 and 19 show how well the valence distributions obtained from the NA10 analysis can describe the data of the E615 experiment by only varying the normalization parameter K'_{252}. The parameters in parentheses are held fixed during each fit.

Fit	α	β	A_s	η_s	η_g	K'_{252}	χ^2/No. of data
18	(0.64)	(1.08)	(0.9)	(5.0)	(2.1)	1.08	102/78
19	(0.64)	(1.08)	(0.9)	(5.0)	(2.1)	1.06	61/61

TABLE VI. Fit 20 shows how well the valence distributions obtained from the E615 analysis can describe the data of the NA10 experiment by only varying the normalization parameters K'_{194} and K'_{286}. The parameters in parentheses are held fixed during each fit.

Fit	α	β	A_s	η_s	η_g	K'_{194}	K'_{286}	χ^2/No. of data
20	(0.64)	(1.15)	(0.9)	(5.0)	(2.1)	1.37	1.43	66/62

TABLE VII. The optimum choice of parameters of the pion distributions derived from all the various fits to the NA10 and E615 Drell-Yan data, together with the fits to the WA70 prompt photon data as described in Sec. III.

Expt.	α	β	A_s	η_s	η_g
NA10	0.64±0.03	1.08±0.02	0.9±0.3	5.0	2.1±0.4
E615	0.64±0.03	1.15±0.02	0.9±0.3	5.0	2.1±0.4

tors. The results of these fits can be seen in Tables V and VI. It appears that the main difference between the NA10 and E615 data sets is one of normalization, as reflected in the difference between the K' factors.

As a result of all of the fits to, in turn, two different data sets, we see that a consistent value of the parameter α is obtained, but that the parameter β differs slightly according to whether the NA10 or E615 data are used. We find that $\alpha=0.64\pm0.03$ for both the NA10 and E615 data, but that $\beta=1.08\pm0.02$ for NA10, whereas $\beta=1.15\pm0.02$ for E615. For reference these parameter values are collected in Table VII; the resulting description of the NA10 and E615 Drell-Yan data is shown in Figs. 3, 4, and 5, while Fig. 6 compares the two sets of parton distributions at $Q^2=5$ GeV^2.

We note that the errors quoted above do not include those due to the uncertainties in the proton distributions. In order to explore the effect of changing these distributions we use the four sets of partons (B135, B160, B200, B235) of Ref. [12]. These four sets span the range of acceptable proton distributions and each corresponds to a different value of $\Lambda^{(4)}_{\overline{\rm MS}}$, namely,

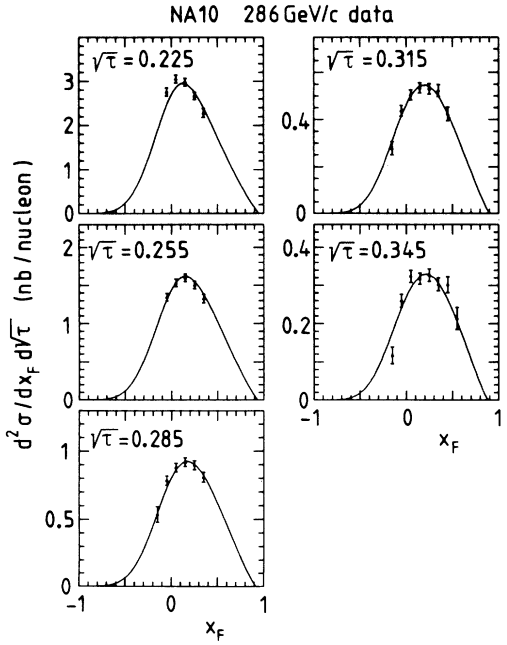

FIG. 4. Drell-Yan data from the NA10 Collaboration [10] for 286 GeV/c π^- on W, together with their description in terms of the NA10 parton distributions of Table VII. The points with $x_F<0$ are not included in the fit.

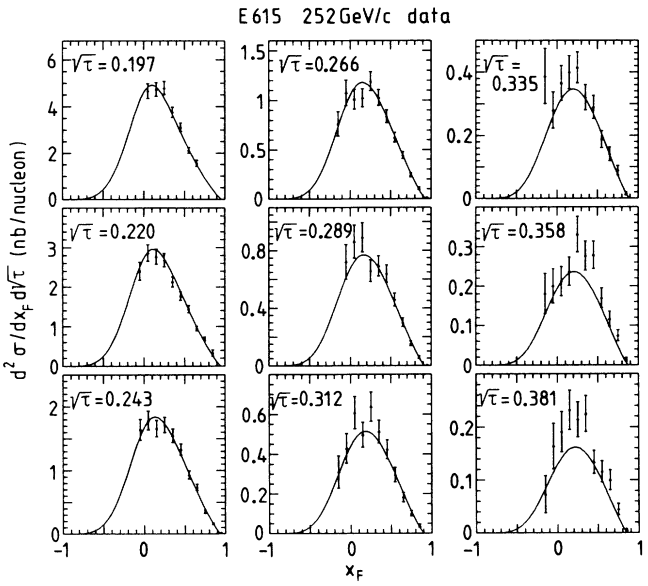

FIG. 5. Drell-Yan data from the E615 Collaboration [6] for 252 GeV/c π^- on W, together with their description in terms of the E615 parton distributions of Table VII. The points with $x_F<0$ are not included in the fit.

$$\Lambda^{(4)}_{\overline{\rm MS}}=135,160,200,235\ \text{MeV}\ .$$

We find from the resulting fits to the NA10 data that the optimum value of α varies between 0.62 and 0.64. It therefore remains within the error determined from the fits that use the HMRS(B) set of partons. The value of β increases from 1.07 to 1.12 as the choice of proton distributions varies from B235 to B135 (and $\Lambda^{(4)}_{\overline{\rm MS}}$ decreases). However, it is clear that the uncertainty in β is still dominated by the disagreement between the two different sets of Drell-Yan data. None of the results of the following sections are particularly sensitive to this small difference

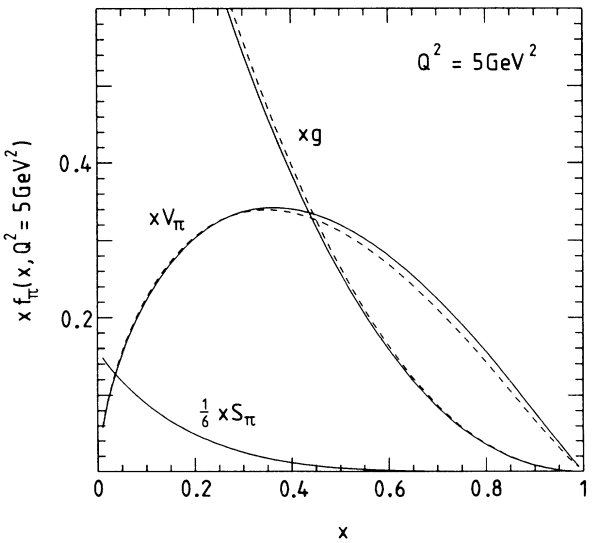

FIG. 6. The parton distributions of Table VII obtained from the fits to the NA10 (solid curves) and E615 (dashed curves) Drell-Yan data evolved to $Q^2=5$ GeV^2.

in β. That is to say, they do not change beyond their quoted errors. We, therefore, use the valence parameters from our NA10 analysis in what follows. We give preference to the NA10 data not only because it has higher statistics, but also because it was the NA10 Collaboration which measured the function R. It thus seems more consistent to use their data. Although E615 has data points at higher values of x_F, these correspond to lower values of x_N where the form of R has not been measured.

III. THE GLUON DISTRIBUTION

The Drell-Yan data do not put any effective constraints on the shape of the gluon distribution of the pion. The gluon dependence only enters at next-to-leading order and even this contribution is considerably smaller than those arising from the other next-to-leading-order processes. By contrast the gluon enters at leading order in the prompt photon processes, $\pi^{\pm}p \to \gamma X$. Moreover, in $\pi^+ p \to \gamma X$, the $gq \to \gamma g$ contribution to the cross section is large, if not larger, than that of the $q\bar{q} \to \gamma g$ annihilation diagrams. We determine the gluon distribution of the pion from the data of the CERN WA70 [13] prompt photon experiment. The valence quarks are held fixed at the values determined by the NA10 Drell-Yan data. The calculation of the cross section for prompt photon production is then performed beyond leading order using the "principle of minimal sensitivity" to determine the optimized factorization and renormalization scales as described in Ref. [14]. Figure 7 shows, in terms of contours of constant χ^2, the quality of the combined fit to the WA70 π^+ and π^- data as a function of $\langle xg \rangle$ and η_g. Now in the proton the gluons are known to carry about 50% of the momentum at $Q^2 = Q_0^2 = 4$ GeV^2. However,

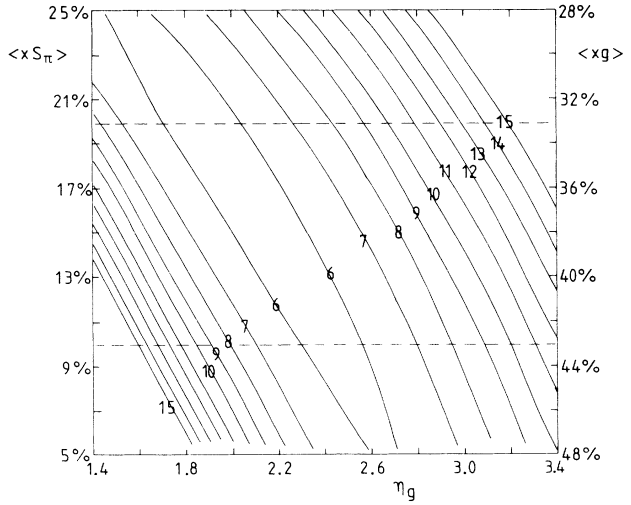

FIG. 7. Contours of constant χ^2 (with values a unit apart) in the plane of $\langle xg \rangle$ and η_g. χ^2 measures the quality of the description of the WA70 prompt photon data $\pi^+ p \to \gamma X$ and $\pi^- p \to \gamma X$ using the valence distributions of Table VII obtained by fitting to the NA10 Drell-Yan data. The valence quarks carry about 47% of the pion momentum; the left- and right-hand vertical scales show the fraction carried by the sea and gluon, respectively. The preferred region lies between the dashed lines.

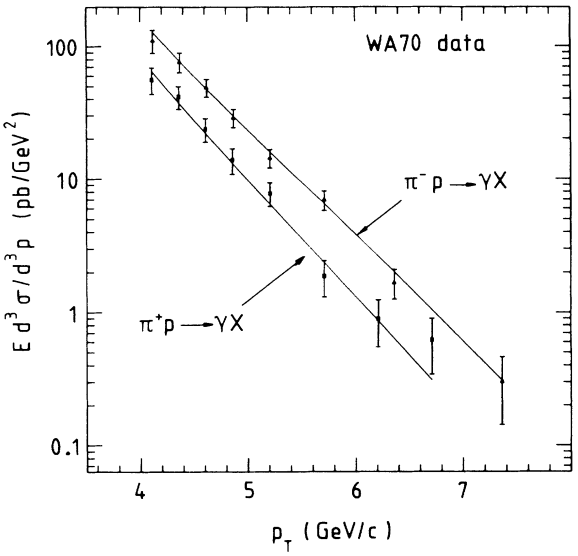

FIG. 8. Data on the transverse-momentum distribution of the photon produced in $\pi^{\pm}p$ collisions at $\sqrt{s} = 22.94$ GeV from the WA70 Collaboration [13] (corrected to $y = 0$) together with the description obtained using the parton distributions from our NA10 and WA70 fits of Table VII.

for a pion, the valence quarks themselves carry $2\alpha/(\alpha+\beta+1) \simeq 47\%$ of its momentum at this Q^2. We have found that a sea-quark distribution carrying only 5% of the pion momentum gives an unacceptable fit to the NA10 Drell-Yan data (see, for example, set 2 of Table I), so we make the reasonable assumption that the sea quarks carry between 10% and 20% of the pion's momentum, and correspondingly the gluon must carry between 43% and 33% of the momentum. (This is con-

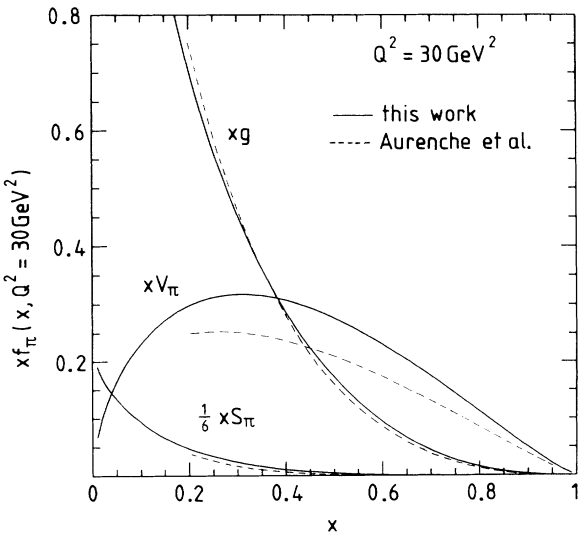

FIG. 9. A comparison of the pion distributions at $Q^2 = 30$ GeV^2 of Ref. [5] with the equivalent distributions of Table VII which are obtained by fitting to the NA10 Drell-Yan data and WA70 prompt photon production data.

sistent with the original measurement of NA3 [2], who found $\langle xg \rangle = 0.47 \pm 0.15$.) We can see from Fig. 7 that if we impose the above limit on $\langle xg \rangle$ then the value of η_g which best describes the prompt photon data is $\eta_g = 2.1 \pm 0.4$. Figure 8 shows the fit to the WA70 prompt photon data obtained using $\eta_g = 2.1$. Although the $\pi^- p \to \gamma X$ data do not constrain the gluon, they do serve as a consistency test of the quark distributions obtained from the Drell-Yan data.

An independent determination of the gluon from WA70 data has been made by Aurenche *et al.* [5] using a different choice of proton distributions. Their results are based purely on an analysis of the prompt photon data and thus rely on earlier, and simpler, analyses of Drell-Yan data for the values of certain valence- and sea-quark parameters. For example, they keep the value of β fixed at 0.85 whereas our analysis favors a larger value ($\beta \simeq 1.1$). For completeness we compare their pion distributions with ours in Fig. 9.

IV. THE SEA DISTRIBUTION

So far we have seen that the valence-quark distribution of the pion, and the exponent η_g of the gluon, are fairly well constrained by Drell-Yan and prompt photon data. The outstanding ambiguity is the size and form of the sea-quark distribution of the pion. Owens [3] assumed that the sea carried a fraction 0.15 of the momentum of the pion with a $(1-x)^{\eta_s}$ "starting" distribution at $Q_0^2 = 4$ GeV^2 with $\eta_s = 5$. This value of η_s is to be expected from naive-spectator quark-counting arguments. The NA3 Collaboration [2], found that their $\pi N \to \mu^+ \mu^- X$ data were compatible with a pion sea which carried momentum fraction 0.19, with $\eta_s = 8.4$ at $Q_0^2 \sim 20$ GeV^2. An advantage of the NA3 experiment was the use of π^+ as well as π^- beams. Although the valence distributions of both pions are the same from isospin symmetry, they contribute to the Drell-Yan process differently through the factors of the quark charge squared. However, unlike the proton, where deep-inelastic-scattering data exist down to $x_N \simeq 0.03$, the pion data exist only for $x_\pi \gtrsim 0.2$. Unfortunately it is not consistent for us to assume that the sea takes the same form as that of the NA3 parametrization. This is because of the different theoretical inputs used by NA3. Figure 10 shows the distribution $u(x,Q^2)+\bar{u}(x,Q^2)$ as given by the NA3 Collaboration at $Q^2 = 20$ GeV^2 compared with our distribution for which we include a range of sea distributions. It is clear that the NA3 quark distributions have a very different form and so it would be meaningless to attempt to incorporate their sea distribution in our analysis. As the NA3 data has never been fully published it is not possible to reanalyze their measured cross sections to extract a consistent sea distribution. Fortunately, we have seen above that the sea has relatively little influence on our determination of the valence quark parameters α and β. As we noted in the previous section, the main uncertainty in η_g arises through our lack of knowledge of how the remaining momentum is divided between the sea and gluons (see Fig. 7). We have imposed reasonable bounds on this division and varied the sea accordingly. The

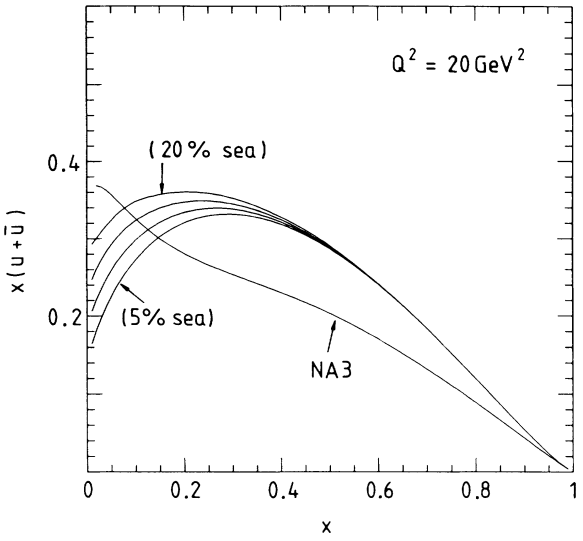

FIG. 10. A comparison of the NA3 [2] parton distribution $u(x,Q^2)+\bar{u}(x,Q^2)$ at $Q^2 = 20$ GeV^2 with the equivalent distributions of Table VII which were fitted to the NA10 Drell-Yan data. The effect of varying the sea-quark distribution is shown.

effect of the variation of the sea is shown in Fig. 10. Further experiments with high-statistics π^+ and π^- beams, ideally with data below $x_\pi \sim 0.2$, are needed in order to more accurately determine the pion sea.

V. PION MOMENTS

In order to compare with lattice QCD calculations we calculate the first two moments of the pion valence-quark distributions:

$$2\langle xV_\pi \rangle = 2\int_0^1 dx\, xV_\pi \,, \tag{9}$$

$$2\langle x^2 V_\pi \rangle = 2\int_0^1 dx\, x^2 V_\pi \,. \tag{10}$$

The Q^2 dependence of these moments for the distributions of Table VII obtained from the NA10 data can be seen in Fig. 11. At $Q^2 = Q_0^2 = 4$ GeV^2 we have $xV_\pi = A_V x^\alpha (1-x)^\beta$ and thus

$$2\langle xV_\pi \rangle \Big|_{Q^2=Q_0^2} = \frac{2\alpha}{\alpha+\beta+1} \,, \tag{11}$$

$$2\langle x^2 V_\pi \rangle \Big|_{Q^2=Q_0^2} = \frac{2\alpha(\alpha+1)}{(\alpha+\beta+1)(\alpha+\beta+2)} \,. \tag{12}$$

Equations (11) and (12) show that the moments are more sensitive to the uncertainty in α than in β.

The first two moments have also been calculated from first principles using lattice QCD [15]. The values at $Q^2 = 49$ GeV^2 are

$$2\langle xV_\pi \rangle = 0.46 \pm 0.07, \quad 2\langle x^2 V_\pi \rangle = 0.18 \pm 0.05 \,. \tag{13}$$

This is to be compared with our values

$$2\langle xV_\pi \rangle = 0.40 \pm 0.02, \quad 2\langle x^2 V_\pi \rangle = 0.16 \pm 0.01 \tag{14}$$

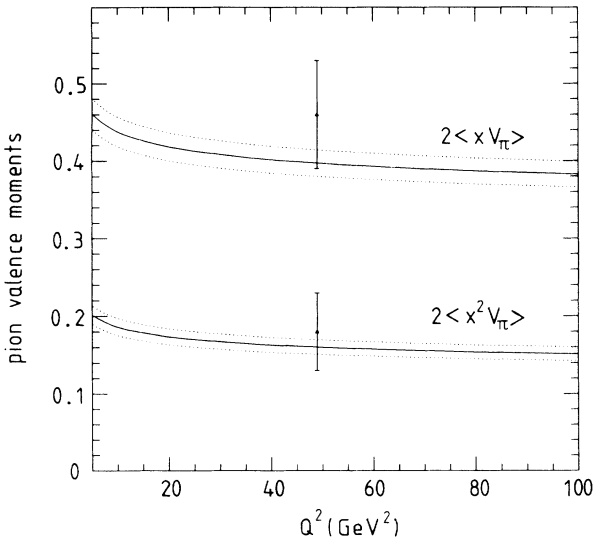

FIG. 11. The first two moments of the pion valence distribution (solid lines) as predicted from the fit to the Drell-Yan data of NA10 compared with the predictions of lattice QCD [15]. The uncertainty in the valence parameters marks out the regions bounded by the dotted lines.

at the same value of Q^2. The lattice calculation is thus consistent with our phenomenological analysis. It is to be expected that the lattice calculation will be higher than the experimental result as the lattice calculation uses the quenched approximation and hence does not contain any sea quarks. This means that the valence quarks will carry slightly more of the momentum. This effect is included in the quoted error for the lattice moments [15].

VI. CONCLUSIONS

We have determined the parton distributions of the pion using all the relevant available high-statistics pion data for Drell-Yan and prompt photon production. We perform a next-to-leading-order analysis adopting the same techniques that HMRS [1] used to determine the parton distributions of the proton, except that since we fit to πN data we need to input proton distributions (HMRS) to determine those of the pion.

We find that we are able to obtain a consistent simultaneous description of the NA10 and E615 Drell-Yan data up to normalization factors; the small difference in the parton distributions is shown in Fig. 6. These data primarily determine the valence-quark distribution of the pion, whereas the main constraint on the form of the gluon distribution comes from WA70 data on prompt photon production from $\pi^+ p$ interactions.

Of course due to the absence of deep-inelastic scattering data we would not expect the pion distributions to be so precisely determined as those of the proton. However, the main deficiency is the lack of pion data with $x_\pi \lesssim 0.2$ to pin down the sea-quark distribution. The standard counting rule $(1-x)^5$ form of the sea gives satisfactory fits, but the normalization is not well determined; a sea which carries either a 10% or 20% fraction of the pion momentum at $Q^2=4$ GeV^2 fits the existing data equally well. The fit deteriorates if the fraction is much smaller, and for larger fractions the gluon momentum fraction becomes unacceptably small (recall that the valence quarks carry 47% of the pion's momentum at $Q^2=4$ GeV^2). The ambiguity in the sea has little effect on the determination of the valence-quark distributions, although it contributes to the uncertainty in the determination of the $1-x$ exponent of the gluon, $\eta_g = 2.1 \pm 0.4$, as shown in Fig. 7.

Three sets of parton distributions of the pion, which span the ambiguity in the sea, are available as a FORTRAN package in the form of (x, Q^2) grids, together with an interpolation routine, from WJS@UK.AC.DURHAM.HEP or from the PDFLIB compilation in the CERN library [16]. These sets are evolved (to next-to-leading order) from initial distributions given by the parameters in Table VIII and correspond to sea-quark distributions carrying 10%, 15%, and

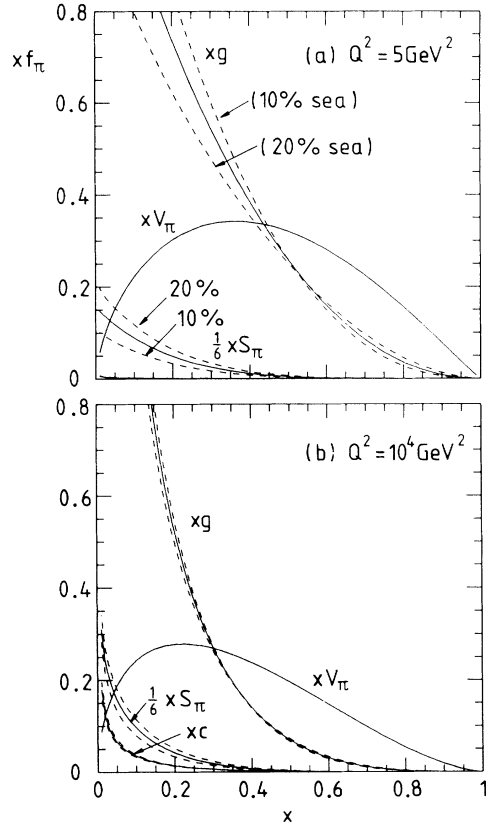

FIG. 12. The parton distributions of Table VIII evolved to (a) $Q^2=5$ GeV^2 and (b) $Q^2=10^4$ GeV^2. The set for which the sea quarks carry 15% of the pion's momentum at $Q^2=4$ GeV^2 is shown as a solid line, and the remaining two sets, for which the sea quarks carry 10% and 20% of the momentum, as dashed lines. The sea-quark distribution is defined as $xS_\pi = 2x(u+\bar{d}+\bar{s})$; also shown is the charm-quark distribution, $xc = x\bar{c}$.

TABLE VIII. The parameters of the initial parton distributions of the pion obtained from fitting NA10 and WA70 data and which correspond, respectively, to the sea quarks carrying 10%, 15%, 20% of the momentum of the pion at $Q^2=4$ GeV^2. The distributions evolved in Q^2 are available as a FORTRAN package as described in the text.

α	β	A_s	η_s	η_g
0.64	1.08	0.6	5.0	2.4
0.64	1.08	0.9	5.0	2.1
0.64	1.08	1.2	5.0	1.8

20% of the momentum of the pion; the central set is the optimum solution (shown in Table VII) which we obtained by fitting to the NA10 Drell-Yan data. Figures 12(a) and 12(b) show these three distributions evolved to $Q^2=5$ GeV^2 and $Q^2=10^4$ GeV^2, respectively.

The pion distributions are useful for future fixed-target physics with pion beams and for (vector-) meson-dominance applications. Finally we note our results are consistent with the QCD lattice computations of the pion distributions.

ACKNOWLEDGMENTS

We thank P. Aurenche and P. Harriman for their valuable help and K. Freudenreich for useful discussions concerning the NA10 Drell-Yan data. One of us (P.J.S.) thanks the UK Science and Engineering Council for financial support.

APPENDIX A

The expressions for the differential cross sections of the Drell-Yan process to order α_s are given in the literature [8] in the deep-inelastic-scattering (DIS) regularization scheme. Here we present the equations for both $d\sigma/dQ^2dx_F$ and $d\sigma/dQ^2dy$ to order α_s in the $\overline{\text{MS}}$ scheme. We separate the expressions into the contributions from $q\bar{q}$ annihilation processes and Compton processes:

$$\frac{d\sigma^A}{dQ^2dx_F}=\frac{4\pi\alpha^2}{9Q^2s}\sum_i e_i^2\int_{x_1}^1 dt_1\int_{x_2}^1 dt_2\left[\frac{d\hat{\sigma}^{\rm DY}}{dQ^2dx_F}+\frac{d\hat{\sigma}^A}{dQ^2dx_F}\right][q_i(t_1,Q^2)\bar{q}_i(t_2,Q^2)+\bar{q}_i(t_1,Q^2)q_i(t_2,Q^2)] \tag{A1}$$

and

$$\frac{d\sigma^C}{dQ^2dx_F}=\frac{4\pi\alpha^2}{9Q^2s}\sum_i e_i^2\int_{x_1}^1 dt_1\int_{x_2}^1 dt_2\left[\frac{d\hat{\sigma}^C}{dQ^2dx_F}g(t_1,Q^2)[q_i(t_2,Q^2)+\bar{q}_i(t_2,Q^2)]+1\leftrightarrow 2\right], \tag{A2}$$

where the leading-order Drell-Yan term in (A1) is

$$\frac{d\hat{\sigma}^{\rm DY}}{dQ^2dx_F}=\frac{1}{x_1+x_2}\delta(t_1-x_1)\delta(t_2-x_2)\ . \tag{A3}$$

The contribution from the order-α_s annihilation graphs is

$$\begin{aligned}\frac{d\hat{\sigma}^A}{dQ^2dx_F}=&\frac{1}{2}A\frac{\delta(t_1-x_1)\delta(t_2-x_2)}{x_1+x_2}\left[-8+\frac{1}{3}\pi^2+\ln^2(1-x_1)+\ln^2(1-x_2)+2\,{\rm Li}_2(x_1)\right.\\&\left.+2\,{\rm Li}_2(x_2)+2\ln\frac{x_1}{1-x_1}\ln\frac{x_2}{1-x_2}\right]\\&+\frac{1}{2}A\frac{\delta(t_2-x_2)}{x_1+x_2}\left[\frac{t_1^2+x_1^2}{t_1^2(t_1-x_1)_+}\ln\frac{(x_1+x_2)(1-x_2)}{x_2(t_1+x_2)}+\frac{1}{t_1}-\frac{x_1}{t_1^2}\right.\\&\left.-\frac{t_1^2+x_1^2}{t_1^2(t_1-x_1)}\ln\frac{x_1}{t_1}+\frac{t_1^2+x_1^2}{t_1^2}\left[\frac{\ln(1-x_1/t_1)}{t_1-x_1}\right]_+\right]\\&+(1\leftrightarrow 2)+\frac{1}{2}A\left[\frac{\tilde{G}^A(t_1,t_2)}{[(t_1-x_1)(t_2-x_2)]_+}+\tilde{H}^A(t_1,t_2)\right],\end{aligned} \tag{A4}$$

where $A=4\alpha_s(Q^2)/3\pi$ and the dilogarithm function ${\rm Li}_2(x)$ is defined by

$${\rm Li}_2(x)=-\int_0^x dt\frac{\ln(1-t)}{t}\ . \tag{A5}$$

The functions $\tilde{G}^A$ and $\tilde{H}^A$ are given by

$$\tilde{G}^{A}(t_1,t_2)=\frac{(t_1+t_2)[\tau^2+(t_1t_2)^2]}{(t_1t_2)^2(t_1+x_2)(t_2+x_1)}\ , \tag{A6}$$

$$\tilde{H}^{A}(t_1,t_2)=\frac{-2}{t_1t_2(t_1+t_2)}\ . \tag{A7}$$

The contribution from the Compton graphs is

$$\frac{d\hat{\sigma}^{C}}{dQ^2dx_F}=\frac{3}{16}A\frac{\delta(t_2-x_2)}{(x_1+x_2)t_1^3}\left[[x_1^2+(t_1-x_1)^2]\ln\frac{(x_1+x_2)(1-x_2)(t_1-x_1)}{x_1x_2(t_1+x_2)}+t_1^2\right]+\frac{3}{16}A\left[\frac{\tilde{G}^{C}(t_1,t_2)}{(t_2-x_2)_+}+\tilde{H}^{C}(t_1,t_2)\right], \tag{A8}$$

with

$$\tilde{G}^{C}(t_1,t_2)=\frac{\tau^2+(t_1t_2-\tau)^2}{t_1^3t_2^2(t_2+x_1)}\ , \tag{A9}$$

$$\tilde{H}^{C}(t_1,t_2)=\frac{1}{(t_1t_2)^2(t_1+t_2)^2}[t_1(t_2+x_1)(t_2-x_2)+2\tau(t_1+t_2)]\ . \tag{A10}$$

The + distributions are defined by

$$\int_x^1 dt\frac{f(t)}{(t-x)_+}=\int_x^1 dt\frac{f(t)-f(x)}{t-x}\ , \tag{A11}$$

$$\int_x^1 dt\, f(t)\left[\frac{\ln(1-x/t)}{t-x}\right]_+=\int_x^1 dt[f(t)-f(x)]\left[\frac{\ln(1-x/t)}{t-x}\right], \tag{A12}$$

and

$$\int_{x_1}^1 dt_1\int_{x_2}^1 dt_2\frac{f(t_1,t_2)}{[(t_1-x_1)(t_2-x_2)]_+}=\int_{x_1}^1 dt_1\int_{x_2}^1 dt_2\frac{f(t_1,t_2)-f(t_1,x_2)-f(x_1,t_2)+f(x_1,x_2)}{(t_1-x_1)(t_2-x_2)}\ . \tag{A13}$$

Similarly for $d\sigma/dQ^2dy$ we have

$$\frac{d\sigma^{A}}{dQ^2dy}=\frac{4\pi\alpha^2}{9Q^2s}\sum_i e_i^2\int_{x_1}^1 dt_1\int_{x_2}^1 dt_2\left[\frac{d\hat{\sigma}^{\rm DY}}{dQ^2dy}+\frac{d\hat{\sigma}^{A}}{dQ^2dy}\right][q_i(t_1,Q^2)\bar{q}_i(t_2,Q^2)+\bar{q}_i(t_1,Q^2)q_i(t_2,Q^2)] \tag{A14}$$

and

$$\frac{d\sigma^{C}}{dQ^2dy}=\frac{4\pi\alpha^2}{9Q^2s}\sum_i e_i^2\int_{x_1}^1 dt_1\int_{x_2}^1 dt_2\left[\frac{d\hat{\sigma}^{C}}{dQ^2dy}g(t_1,Q^2)[q_i(t_2,Q^2)+\bar{q}_i(t_2,Q^2)]+1\leftrightarrow 2\right], \tag{A15}$$

where now the leading-order Drell-Yan term in (A14) is

$$\frac{d\hat{\sigma}^{\rm DY}}{dQ^2dy}=\delta(t_1-x_1)\delta(t_2-x_2)\ . \tag{A16}$$

The contribution from the order-α_s annihilation graphs is

$$\begin{aligned}\frac{d\hat{\sigma}^{A}}{dQ^2dy}=&\frac{1}{2}A\delta(t_1-x_1)\delta(t_2-x_2)\left[-8+\frac{1}{3}\pi^2+\ln^2(1-x_1)+\ln^2(1-x_2)+2\,\mathrm{Li}_2(x_1)+2\,\mathrm{Li}_2(x_2)+2\ln\frac{x_1}{1-x_1}\ln\frac{x_2}{1-x_2}\right]\\&+\frac{1}{2}A\delta(t_2-x_2)\left[\frac{t_1^2+x_1^2}{t_1^2(t_1-x_1)_+}\ln\frac{2x_1(1-x_2)}{x_2(t_1+x_1)}+\frac{1}{t_1}-\frac{x_1}{t_1^2}-\frac{t_1^2+x_1^2}{t_1^2(t_1-x_1)}\ln\frac{x_1}{t_1}+\frac{t_1^2+x_1^2}{t_1^2}\left[\frac{\ln(1-x_1/t_1)}{t_1-x_1}\right]_+\right]\\&+(1\leftrightarrow 2)+A\left[\frac{G^{A}(t_1,t_2)}{[(t_1-x_1)(t_2-x_2)]_+}+H^{A}(t_1,t_2)\right],\end{aligned} \tag{A17}$$

where the functions G^{A} and H^{A} are given by

$$G^{A}(t_1,t_2)=\frac{(\tau+t_1t_2)[\tau^2+(t_1t_2)^2]}{(t_1t_2)^2(t_1+x_1)(t_2+x_2)}\ , \tag{A18}$$

$$H^A(t_1,t_2)=\frac{-2\tau(\tau+t_1t_2)}{t_1t_2(t_1x_2+t_2x_1)^2} . \tag{A19}$$

The contribution from the Compton graphs is

$$\frac{d\hat{\sigma}^C}{dQ^2dy}=\frac{3}{8}A\delta(t_2-x_2)\left[\frac{x_1^2+(t_1-x_1)^2}{2t_1^3}\ln\frac{2(1-x_2)(t_1-x_1)}{x_2(t_1+x_1)}+\frac{1}{2t_1}\right]+\frac{3}{8}A\left[\frac{G^C(t_1,t_2)}{(t_2-x_2)_+}+H^C(t_1,t_2)\right] , \tag{A20}$$

with

$$G^C(t_1,t_2)=\frac{x_2(\tau+t_1t_2)[\tau^2+(\tau-t_1t_2)^2]}{t_1^3t_2^2(t_1x_2+t_2x_1)(t_2+x_2)} , \tag{A21}$$

$$H^C(t_1,t_2)=\frac{\tau(\tau+t_1t_2)[t_1t_2^2x_1+\tau(t_1x_2+2t_2x_1)]}{(t_1t_2)^2(t_1x_2+t_2x_1)^3} , \tag{A22}$$

and $A=4\alpha_s(Q^2)/3\pi$ as before.

[1] P. N. Harriman, A. D. Martin, W. J. Stirling, and R. G. Roberts, Phys. Rev. D **42**, 798 (1990) (HMRS); M. Diemoz, F. Ferroni, E. Longo, and G. Martinelli, Z. Phys. C **39**, 21 (1988); P. Aurenche, R. Baier, M. Fontannaz, J. F. Owens, and M. Werlen, Phys. Rev. D **39**, 3275 (1989); J. Kwiecinski, A. D. Martin, W. J. Stirling, and R. G. Roberts, *ibid.* **42**, 3645 (1990); J. Morfin and Wu-ki Tung, Z. Phys. C **52**, 13 (1991).

[2] NA3 Collaboration, J. Badier *et al.*, Z. Phys. C **18**, 281 (1983).

[3] J. F. Owens, Phys. Rev. D **30**, 943 (1984).

[4] NA10 Collaboration, B. Betev *et al.*, Z. Phys. C **28**, 15 (1985).

[5] P. Aurenche, R. Baier, M. Fontannaz, M. N. Kienzle-Focacci, and M. Werlen, Phys. Lett. B **233**, 517 (1989).

[6] E615 Collaboration, J. S. Conway *et al.*, Phys. Rev. D **39**, 92 (1989).

[7] R. Hamberg, W. L. van Neerven, and T. Matsuura, Nucl. Phys. **B359**, 343 (1991).

[8] J. Kubar, M. Le Bellac, J. L. Meunier, and G. Plaut, Nucl. Phys. **B175**, 251 (1980).

[9] NA10 Collaboration, P. Bordalo *et al.*, Phys. Lett. B **193**, 368 (1987).

[10] NA10 Collaboration, B. Betev *et al.*, Z. Phys. C **28**, 9 (1985). Note that the cross sections in this paper have since been revised with a better estimate of Fermi motion effects; see, for example, [11].

[11] K. Freudenreich, Int. J. Mod. Phys. A **19**, 3643 (1990).

[12] A. D. Martin, R. G. Roberts, and W. J. Stirling, Phys. Rev. D **43**, 3648 (1991).

[13] WA70 Collaboration, M. Bonesini *et al.*, Z. Phys. C **37**, 535 (1988).

[14] P. M. Stevenson and H. D. Politzer, Nucl. Phys. **B277**, 758 (1986).

[15] G. Martinelli and C. T. Sachrajda, Nucl. Phys. **B306**, 865 (1988).

[16] H. Plothow-Besch, in *Proceedings of the 3rd Workshop on Detector and Event Simulation in High Energy Physics,* Amsterdam, 1991, edited by K. Bos and B. van Eijk (NIKHEF-H, Amsterdam), p. 148.